Solid-State Electronics 191 (2022) 108262

Contents lists available at ScienceDirect

Solid State Electronics

journal homepage: www.elsevier.com/locate/sse

Phenomenological modeling of low-bias sulfur hexafluoride plasma etching of silicon

Luiz Felipe Aguinsky [a,*,1], Frâncio Rodrigues [a,1], Georg Wachter [b], Michael Trupke [b], Ulrich Schmid [c], Andreas Hössinger [d], Josef Weinbub [a]

[a] Christian Doppler Laboratory for High Performance TCAD, Institute for Microelectronics, TU Wien, Gußhausstraße 27-29, 1040 Wien, Austria
[b] Faculty of Physics, University of Vienna, VCQ, Boltzmanngasse 5, 1090 Wien, Austria
[c] Institute of Sensor and Actuator Systems, TU Wien, Gußhausstraße 27-29, 1040 Wien, Austria
[d] Silvaco Europe Ltd., Compass Point, St Ives, Cambridge, PE27 5JL, United Kingdom

ARTICLE INFO

Keywords:
SF_6 plasma etching
Topography simulations
Microfabrication
Isotropic etching
Optical devices
MEMS

ABSTRACT

Low-bias etching of silicon (Si) using sulfur hexafluoride (SF_6) plasma is a valuable tool in the manufacturing of electronic devices and microelectromechanical systems (MEMS). This kind of etching offers an almost isotropic etching behaviour, since the low voltage bias does not provide enough vertical acceleration and kinetic energy to the ions. Due to this near-isotropic behavior, the aforementioned plasma etching finds application as an alternative to wet etching in, e.g., MEMS and optical applications since it provides a cleaner and more precisely controllable process. However, the degree of isotropy and, consequently, the final surface profile remain difficult to control. In this work, we apply a three-dimensional feature-scale topography simulation to low-bias SF_6 etching experiments in Si to aid in process development and to investigate the physical etching mechanisms which govern the final surface geometry. We achieve this by accurately reproducing three distinct experimental data sets and by discussing the meaning of the phenomenological model parameters involved in the topography simulation in detail. We show that our phenomenological top-down flux calculation approach more accurately reproduces the experimental results than conventional strictly isotropic and bottom-up approaches. The reactor loading effect is taken into account as a general reduction of the model etch rates, which is supported by comparing simulated to experimentally determined etch depths in different loading regimes. Our model is also able to accurately reproduce reported trench geometries for different mask openings and etch times using a single parameter set for a given reactor configuration. Hence, we propose that the model parameters, in particular the average effective sticking coefficient, can be taken as a proxy of the reactor configuration. We provide an empirical relationship linking the average sticking coefficient of a reactor recipe to a measurable degree of isotropy of etched geometries. This empirical relationship can be used in practice to (i) estimate the average effective sticking coefficient of independent experiments and to (ii) fine-tune the etched geometry.

1. Introduction

Plasma etching of silicon (Si) using sulphur hexafluoride (SF_6) gases is a standard technology in modern microfabrication processes [1], with applications such as memory devices, microelectromechanical systems (MEMS), and as a sub-step in the Bosch process [2,3]. Under low-bias conditions, SF_6 plasma etching is known to have a near-isotropic behavior yielding profiles similar, but not identical, to those obtained by isotropic wet etching [4]. This is due to the low voltage bias between the plasma and the wafer not accelerating the ions to a large degree. Therefore, the anisotropic component, caused by the kinetic energy of the vertically impinging ions, is minimal [5]. The near-isotropic behavior has proven to be useful in, e.g., optical applications, where surface cleanliness requirements favor plasma etching over wet etching [6]. Furthermore, in MEMS applications, the surface tension of wet etchants can lead to damage of the involved layers and membranes at the micro- and nano-scale [7]. In addition, plasma etching provides advantages with respect to controllability, reproducibility, and

* Corresponding author.
E-mail address: aguinsky@iue.tuwien.ac.at (L.F. Aguinsky).
[1] These two authors contributed equally to this work.

https://doi.org/10.1016/j.sse.2022.108262
Received 10 November 2021; Received in revised form 28 January 2022; Accepted 21 February 2022
Available online 25 February 2022

uniformity.

At first, plasma etching of Si was proposed using fluorine gas (F_2) [8] and xenon difluoride (XeF_2) [9]. These processes yield isotropic etch characteristics and XeF_2 etching in particular has been recently applied for the realization of on-chip cooling microchannels [10] and for the development of MEMS sacrificial layers [7]. However, XeF_2 reacts with moisture to form hydrofluoric acid (HF) [11], which etches silica (SiO_2) [4], imposing selectivity restrictions when using SiO_2 masks. In addition, etching with XeF_2 is an expensive process that requires specially designed equipment which has not been integrated with complementary metal–oxide–semiconductor (CMOS) fabrication processes [4]. Out of the many fluorinated gases, SF_6 is frequently used due to its inert nature and superior etch rate [12]. Thus, SF_6 etching of Si has been established as a preferred, CMOS-compatible method.

Although these higher etch rates and reaction probabilities are important for high-throughput industrial applications, they can lead to complications if isotropic etch characteristics are desired. Notwithstanding, significant progress has been made since low-bias SF_6 etching of Si has been proposed for Si microlens mold fabrication [13]. Critical work has been done to control the roughness of the final surface [14,15], leading to the development of high-finesse optical resonator cavities [6].

The final shapes of the etched surfaces are not straightforwardly predicted since the process is not perfectly isotropic. This has lead to the definition of a quantitative metric of isotropy [4] and its measurement in patterned features. Those results indicate that SF_6 can be used in a variety of applications as a replacement for wet etching or for a complex etch chemistry such as XeF_2. The question of how to control the isotropy and thus the final shape, remains under investigation.

We tend to this knowledge gap by developing a topography simulation with a phenomenological surface model and calibrating it to experimental data. Feature-scale topography simulations are part of process technology computer-aided design (TCAD) workflows which enable, among others, the investigation of etched or deposited materials [16]. Two-dimensional feature-scale modeling of SF_6 etching of Si has been reported for anisotropic, high-bias conditions [17]. In the low-bias regime, a different set of challenges for accurately modeling the topography occurs. Recently, we have proposed a three-dimensional feature-scale simulation for low-bias SF_6 etching of Si [18] including a robust calibration procedure and applied it to the optimization of the fabrication of optical microcavity resonators. Nevertheless, this model involves a quantity which is not readily available: the sticking coefficient β, a measurement of the reaction probability between reactants and the surface. It is a necessary parameter to calculate etchant flux values while taking into account reflections of impinging values. However, β values are challenging to measure, and vary over a wide range depending on specific experimental conditions in ways which are still under investigation [19,20].

In this work, we expand the physical interpretation of the phenomenological surface model involved in the feature-scale topography simulation with a top-down approach, in particular discussing the role of sticking coefficients (Section 2). The model results are shown and discussed in detail in Section 3 in multiple manners. Our model is contrasted to conventional, strictly isotropic, and bottom-up models [21] in their ability to replicate experimentally measured cavities. The role of the reactor loading effect is then discussed as it relates to the capabilities of the model. We calibrate our model to two data sets of etched trenches reported in the literature [13,4], highlighting the capability of our model to reproduce multiple geometries and etch times with a single parameter set for each different reactor configuration. With this insight, we propose that the isotropy, which is a measurable quantity, can be used to estimate the average effective sticking coefficient, thereby effectively characterizing the reactor configuration.

2. Methods

2.1. Topography simulation

In order to simulate the three-dimensional time evolution of an etched surface, we employ the level-set method [22]. The evolving surface is represented as the zero level-set of the signed distance function ϕ. Its propagation is described by the solution of the following level-set equation for ϕ:

$$\frac{\partial \phi(x,t)}{\partial t} + ER\left(x\right)\left|\nabla \phi\left(x,t\right)\right| = 0. \tag{1}$$

The modeling of surface reactions and subsequent local etch rates is achieved via the local etch rate field $ER(x)$, as discussed below. The solution of (1) is performed by Silvaco's three-dimensional process TCAD tool *Victory Process* [23] and by the open-source topography simulator *ViennaTS* [24]. In Fig. 1, we present a two-dimensional illustration of three possible approaches to generate $ER(x)$ for an isotropic etchant.

As reported previously [1], under low-bias conditions the etching is expected to be near-isotropic. Such etching is mostly performed by highly reactive isotropic F radicals generated in the plasma. The lack of energetic ions also improves etch selectivity of Si over photoresist or hardmask [25]. Due to the low-bias, the directional component caused by the vertically accelerated ions is minimal.

The precise nature of the low-bias behavior requires accurate modelling. The straightforward approach, i.e., strictly isotropic, is represented in Fig. 1.a). In this case, the same constant etch rate is applied to all exposed surface elements of the same material. This results in a surface equivalent to that processed by ideal isotropic wet etching [26].

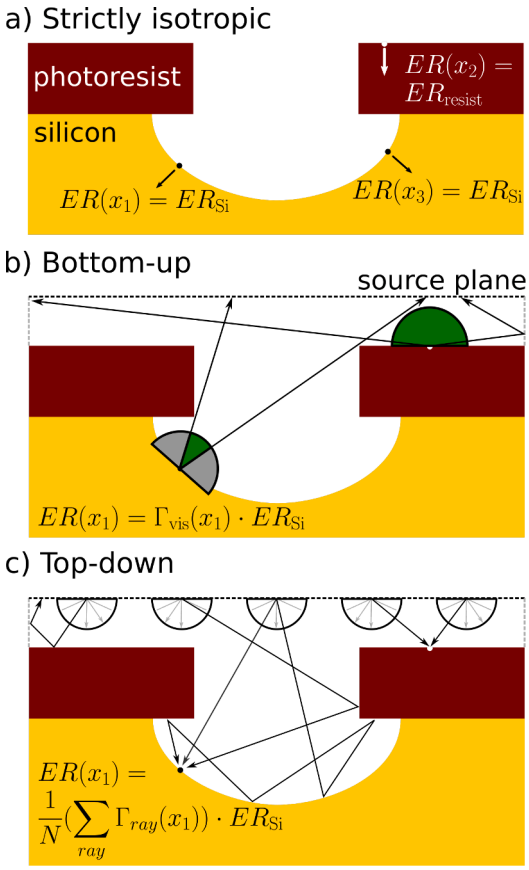

Fig. 1. Illustration of models for the local etch rate $ER(x)$. Our top-down model (c) is contrasted to the conventional strictly isotropic (a) and bottom-up (b) procedures.

Therefore, in the strictly isotropic case the etch rate $ER_{S-I}(x)$ is simply a function of the involved material (in this example, either Si or the resist):

$$ER_{S-I}(x) = ER_{Si/resist}. \quad (2)$$

However, since plasma etching is a gas-phase method, the etchant distribution is not always identical across the surface. A more complex model thus requires the construction of an approximation to the local flux of etchant particles $\Gamma(x)$ in order to more accurately model $ER(x)$. An elementary approach to calculating $\Gamma(x)$, represented in Fig. 1.b), assumes that the incoming particle stream originates isotropically from a source plane. Subsequently, the local visibility of this plane is calculated in a bottom-up fashion for the hemisphere above each surface element [21], leading to a local flux $\Gamma_{vis}(x)$ which is normalized to 1 for a fully-exposed element. The final etch rate is the plane-wafer etch rate weighted with $\Gamma_{vis}(x)$. This model allows the capture of some topography-dependent effects, however, it does not take reflections of impinging particles into account. The etch rate field in the bottom-up model $ER_{B-U}(x)$ is:

$$ER_{B-U}(x) = \Gamma_{vis}(x) \cdot ER_{Si/resist}. \quad (3)$$

We propose a physically richer top-down model, as shown in Fig. 1. c), supporting multiple reflections according to the sticking probability β. This is achieved by a Monte Carlo sampling of multiple particles of a single type, which are generated isotropically in the source plane and carry a flux payload Γ_{ray}. Their trajectories through the domain are computed using a ray-tracing method and reflective boundary conditions. When a simulated particle hits the surface, it is terminated, leaving its payload Γ_{ray} at the surface site. A new reflected particle is generated, following an isotropic reflection distribution and having a new payload Γ_{ref} mediated by $\beta_{Si/resist}$, i.e.:

$$\Gamma_{ref} = (1 - \beta_{Si/resist}) \cdot \Gamma_{ray}. \quad (4)$$

Finally, the local etch rate of the surface is calculated from the normalized sum of $\Gamma_{ray}(x)$ for all particles, both generated in the source plane and reflected, and from the plane-wafer etch rate ER. The normalization constant N is the product of the source plane area and the number of rays generated on the source plane, so that a fully exposed element receives the plane-wafer etch rates. This model effectively generalizes the two previous ones, as the strictly isotropic approach is recovered with the limit $\beta \to 0^+$, and the bottom-up, with $\beta \to 1^-$. In summary, the etch rate for the top-down model ER_{T-D} is:

$$ER_{T-D}\left(x\right) = \frac{1}{N}\left(\sum_{ray} \Gamma_{ray}\left(x\right)\right) \cdot ER_{Si/resist}. \quad (5)$$

The isotropic source and reflection distributions are motivated by the low-bias characteristics of the etching process [27]. As a consequence, the etchants are not accelerated and interact with the surface in a diffuse manner. This is consistent with the expected etching mechanism: The generation of F radicals in the plasma which chemically attack the surface [8].

Therefore, the free parameters are the Si plane-wafer etch rates ER_{Si}, and the photoresist etch rate ER_{resist}. In addition, the top-down model has as parameters the sticking coefficients β_{Si} and β_{resist}. Although this indicates that the top-down model is successful due to its additional fitting parameters, we discuss in Section 3.1 that conventional models require different values of ER_{Si} for each individual initial photoresist geometry, which is not straightforwardly justifiable from a physical standpoint. Thus, the top-down model involves not only an equivalent number of parameters, but also its values can be physically interpreted and compared to reported results [25].

2.2. Physical interpretation of the phenomenological surface model

As discussed above, the top-down model requires two parameters per involved material: $ER_{material}$ and $\beta_{material}$. The physical interpretation of $ER_{material}$ is straightforward, i.e., the plane-wafer etch rate. This is experimentally accessible and is routinely measured. In contrast, the interpretation of the sticking coefficient $\beta_{material}$ is more complex. Sticking coefficients are often a source of confusion in the literature [19], and they are hard to measure experimentally. In our top-down model, $\beta_{material}$ simply represents the fraction of an incoming ray payload that is adsorbed onto a surface element:

$$\Gamma_{ads} = \beta_{material} \cdot \Gamma_{ray}. \quad (6)$$

To understand the physical meaning of β, we analyze it with respect to Langmuir adsorption kinetics models. In a Langmuir model of fluorinated etching of Si, a sticking coefficient is introduced as the reaction probability of an incoming F etchant species adsorbing into the Si surface. The adsorption rate R_{ads} of F in a surface element is given by [17]

$$R_{ads} = S_0(1 - \Theta_F) \cdot \Gamma_F = S_{eff} \cdot \Gamma_F, \quad (7)$$

where S_0 is the sticking coefficient of F on a clean, unfluorinated Si surface, Γ_F is the incoming F flux, and Θ_F is the F local surface coverage. Θ_F represents the fraction of available surface sites occupied by F, thus varies between 0 and 1. $S_{eff}(x) = S_0(1 - \Theta_F)$ is the effective sticking coefficient, its minimum value is 0 and it reaches its maximum value (S_0) when the surface is perfectly clean ($\Theta_F = 0$).

Calculating coverage values introduces several complications and a myriad of new parameters. A more detailed chemical reaction model would also require different clean surface sticking coefficients S_0 for different impinging fluorinated species (e.g., F_2, SF_x). To further complicate matters, the role of S is still under investigation; S might directly catalyze the etch reaction by increasing the sticking coefficient of F [19,20].

In our model we do not calculate neither surface coverages nor consider individual chemical species and reactions. Our single Monte Carlo particle represents a sampling of all the different impinging species present in the reactor. However, our sticking can be seen as an average effective sticking coefficient ($\overline{S_{eff}}$), which captures the effects of surface coverage and of different chemical species in one global parameter. By comparing Eq. (6) to Eq. (7) we achieve:

$$\beta_{Si} \cdot \Gamma_{ray} = \overline{S_{eff}} \cdot \Gamma_F. \quad (8)$$

Eq. (8) provides a useful connection between our phenomenological model to results from surface physics. It defines an expected upper bound, as $\beta_{Si} \leqslant S_0$. Accordingly, β should not exceed the maximum reported value in the literature for Si etched by SF_6, i.e., $S_0 = 0.7$ [17]. It also implies that, with a proper calibration to a given reactor setup, β provides guidance to the global etch reaction probability of the reactor species. As discussed in the following sections, the calibration of our model also utilizes a global plane wafer etch rate $ER_{material}$ that is not tied to any specific chemical species. Hence, both model parameters attempt to capture the global conditions of the reactor, defining our phenomenological modeling to the complex plasma etching phenomena.

3. Results and discussion

3.1. Evaluation of the etch rate model

To evaluate the proposed model, we compare it to three-dimensional profilometer measurements of experimentally fabricated structures [6]. Multiple cavities were etched simultaneously on Si using a two-step SF_6 plasma etching process with the reactor setup shown in Table 1. Each cavity is under a different initial photoresist cylindrical opening d. We studied three different cavities with a respective d of 12.4 μm, 34 μm, and 52 μm. A first etch step was performed for 320 s and took place having the photoresist present. After photoresist removal using acetone, a second etch step was applied for 48 min.

The parameters for the top-down model are obtained with an auto-

Table 1
Reported experimental ICP reactor configurations.

Parameter	Wachter et al. 2019 [6]	Panduranga et al. 2019 [4]	Larsen et al. 2005 [13]
Pressure (*mTorr*)	–	30	10
Flow rate (*sccm*)	100	50	200
Coil power (*kW*)	2	2	3
Table power (*W*)	15	0	0
Chuck temperature (°C)	30	20	20

matic calibration procedure previously developed by us [18] and presented in Table 2. For the strictly isotropic and bottom-up models, the same ER_{resist} and second etch step ER_{Si} are applied, however, each cavity requires a manually calibrated first step ER_{Si}, presented in Table 3. A cross-section contrasting the simulation approaches to the experiment is shown Fig. 2.

The results show the failure of the bottom-up model, since it cannot correctly capture the curvature, i.e., it underestimates the etch rates at the sidewalls. The strictly isotropic model has a very similar shape to the experiment and to the top-down model, in particular for the cavity with $d = 12.4$ µm. However, since it applies the same rate to all exposed regions, the bottom of the cavity, i.e., the area under the original photoresist opening, remains unrealistically flat. Since the strictly isotropic model is equivalent to having $\beta = 0$, the similarity of the strictly isotropic model to the experimental profile is evidence that a low β is expected, as confirmed by the calibrated values in Table 2. However, the perfectly flat profiles at the bottom are not observed in the experiment [6] and, additionally, cause the surface to be unsuited for optical applications and incompatible with further numerical investigation [28].

In addition to the observed correspondence with the experiment shown in Fig. 2, the top-down model offers a significant advantage. Only a single ER_{Si} for the first etch step is required, whereas separate values are required for each cavity for conventional models. This indicates that the top-down model more accurately captures the real chemical processes involved in low-bias SF_6 etching. The calibrated parameters in Table 2 show a lower ER_{Si} for the second etch step. This is expected due to the effect of reactor loading, which is discussed in detail in Section 3.2.

Using topography simulations, we are able to explore states which are not readily available experimentally. In particular, the profile after the first etch step but before photoresist removal, shown in Fig. 3. For the top-down approach, this figure is obtained with the parameters from Table 2. The parameters were re-calibrated for the bottom-up and strictly isotropic models in order to achieve the same depth.

We can see that the bottom-up approach without reflections has fundamental limitations. The shape is more bulbous, which leads to the incorrect final curvature as seen in Fig. 2. Additionally, the bottom-up model without reflections is unable to capture underetching, i.e., the etching of Si directly below the photoresist, which is experimentally a known feature of low-bias SF_6 etching [1]. For the strictly isotropic approach, the flatness of the bottom is even clearer at this step. As discussed previously, this makes the strictly isotropic approach unsuitable. Finally, we would like to highlight that our simulations indicate the presence of photoresist tapering during the etching, which is a phenomenon of interest for further process improvement.

Table 2
Calibrated parameters for top-down simulation [18].

Parameter	Calibrated value
First etch step ER_{Si}	2.15 µm min^{-1}
Second etch step ER_{Si}	0.66 µm min^{-1}
ER_{resist}	0.21 µm min^{-1}
β_{Si}	7.5%
β_{resist}	6.1%

Table 3
Calibrated first etch step 1st ER_{Si} for each photoresist opening d for the strictly isotropic and bottom-up simulations.

d	Strictly isotropic 1st ER_{Si}	Bottom-up 1st ER_{Si}
12.4 µm	1.45 µm min^{-1}	23.0 µm min^{-1}
34 µm	1.94 µm min^{-1}	6.0 µm min^{-1}
52 µm	2.09 µm min^{-1}	3.6 µm min^{-1}

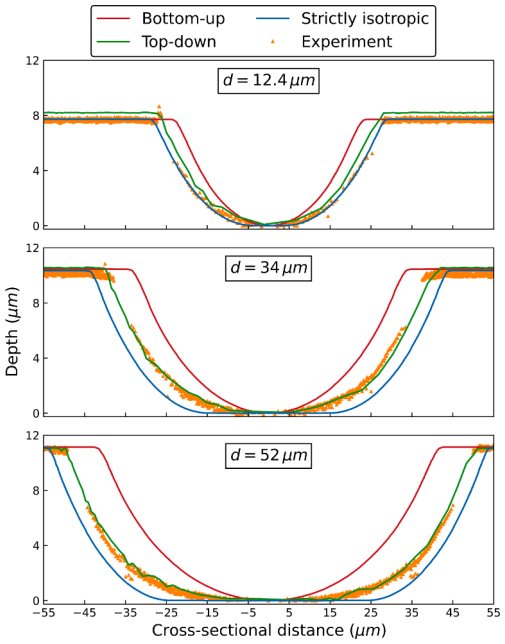

Fig. 2. Cross-sections of the simulated surfaces using the models from Fig. 1 and measurements of experimentally fabricated surfaces with different initial photoresist openings d using a two-step low-bias SF_6 plasma etching process.

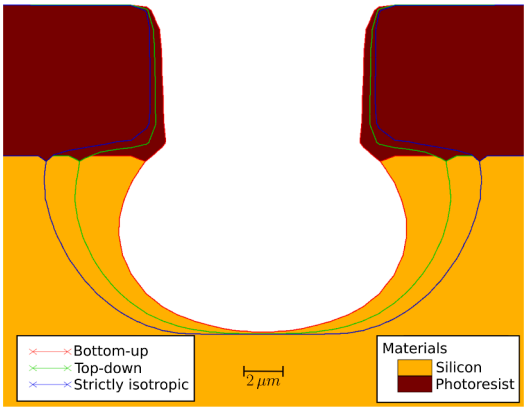

Fig. 3. Simulated etched surfaces for a cavity with photoresist $d = 12.4$ µm showing underetching and photoresist tapering.

3.2. Reactor loading effect

The reactor loading effect is an observed reduction in etch rates due to changes in the exposed wafer surface [1,29]. As the amount of available Si exposed to the reactor increases, for example after removal of the photoresist, there is a diminution of the local amount of available reactants since they are consumed by the larger area. Thus, a reduction

in etch rates is observed even with otherwise identical reactor configurations.

This complicates the development of a general topography simulation for a given reactor configuration, since not only the reactor but the exposed area must be taken into account. We tackle this issue by treating the ER_{Si} as a fitting parameter for each reactor and wafer configuration. This treatment approximates the exposed area as constant during the involved etch step, which is reasonable assuming a low photoresist or hardmask etch rate.

The inclusion of different etch rates due to reactor loading was already shown to be necessary for reproducing the profiles of the two-step cavity etch [6,18], discussed in Section 3.1. In order to validate this approach more generally, we calibrate our simulation to results reported by Panduranga et al. [4]. The authors report etch depths of SF_6 etching of Si using an inductively coupled plasma (ICP) reactor under a large (500 μm diameter) cylindrical hardmask (chromium-on-oxide) opening in two configurations: with a carrier wafer (high loading, lower etch rates) and placed directly on the stainless steel carrier plate (low loading, higher etch rates).

We manually calibrate our simulations by adjusting the plane-wafer etch rate ER_{Si} for each reactor loading configuration until agreement with the reported etch depths is found. The time evolution of these simulations and their comparison to the reported experimental measurements are shown in Fig. 4. Good agreement is observed, supporting our treatment of the ER_{Si} as a different fitting parameter for each configuration. Our calibrated etch rate simulation parameters are shown in Table 4, and they are within the range of experimental values reported in the original work (between 2.07 and 2.47 μm min^{-1} in the low loading regime).

3.3. Etching on trenches

A key advantage of our three-dimensional simulation is that we can evaluate trenches separately to cylindrical holes, whereas two-dimensional simulations cannot distinguish between them. Although both geometries yield equivalent cross-sections, our top-down model results in different local etch rates, since the overall number of incoming particles at each point depends on reflections through the whole geometry. We are thus able to manually calibrate simulations to Si trenches etched with low-bias SF_6 reported in the literature.

Larsen et al. [13] report scanning electron micrography profiles of trenches etched in the same reactor configuration, shown in Table 1, for different photoresist initial openings and etch times t. The initial geometry of the simulations are individual photoresist layers with the same reported heights (1.5 μm) and initial openings (d) and over a slab of Si of dimensions 140 μm × 40 μm, i.e., each trench is simulated individually. The same model parameters are then applied to each

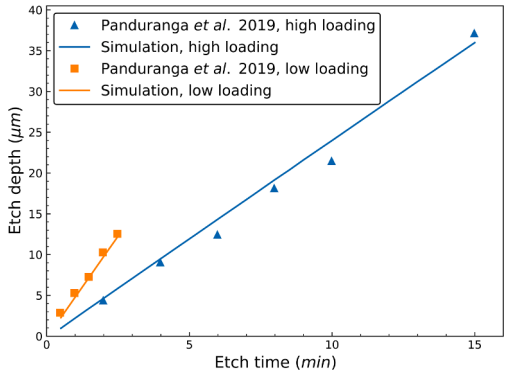

Fig. 4. Comparison of etch depths reported by Panduranga et al. [4] with simulation results in the high and low loading regimes, i.e., with and without a Si carrier wafer respectively.

Table 4
ER_{Si} simulation parameters manually calibrated to experimental etch depths reported by Panduranga et al. [4].

Low loading ER_{Si}	High loading ER_{Si}
4.92 μm min^{-1}	2.40 μm min^{-1}

trench, achieving the cross-sectional profiles shown in Fig. 5. The calibrated parameters are presented in Table 5. The photoresist sticking coefficient was kept the same as the one from the automated calibration [18] in Table 2.

With a single parameter set, we show excellent agreement for values of t below 610s. For higher etch times, our simulations report slightly lower local etch rates as our model does not consider the evolution of the photoresist geometry. The original work reports a micrography of the trench with $d = 7$ μm and $t = 610s$ showing significant photoresist bending due to stress, which is expected to have occurred in all trenches with high etch times. Such bending effectively increases the photoresist opening by almost 1 μm, leading to a marginal increase in flux which is not captured by our model. This difference is not as pronounced in the trench with $d = 62$ μm as the effective increase in opening is small compared to the original opening.

Similarly, Panduranga et al. [4] etch multiple trenches with the reactor setup shown in Table 1, and report etch depths and undercuts measured with a stylus profilometer. We calibrate our simulation to those points, considering the different masking material (0.39 μm layer of chromium-on-oxide hardmask) and keeping the lower plane-wafer etch rate from Table 4, since the authors used a high loading regime for finer process control. The calibrated parameters are presented in Table 6 and the comparison of the simulated geometries to the experimental data is shown in Fig. 6. We note that the reported experimental data exhibits noise due to the measurement accuracy, leading to challenges with regards to calibrating to the measured undercut. Additionally, a comparison of simulated to a scanning electron micrography image for a trench with $d = 8$ μm is shown in Fig. 7.

Our results show that our phenomenological model combined with topography simulation is capable of reproducing etched geometries with only two free parameters per material: plane-wafer etch rates and sticking coefficients. As shown previously in Fig. 4, the plane-wafer etch rates can be estimated by inspecting large features and considering reactor loading effects. The sticking coefficient, however, requires in principle careful calibration in order to correctly reproduce the geometries. Nonetheless, we highlight that a single parameter set is able to reproduce multiple initial geometries and etch times for the same reactor configuration. This is evidence that the sticking coefficient captures in a phenomenological sense the essential characteristics of the reactor configuration and can be taken as a proxy of the reactor recipe.

4. Empirical relationship between degree of isotropy and phenomenological model

Since low-bias SF_6 plasma etching of Si does not yield ideally isotropic profiles, a measurement of the degree of isotropy I has been proposed for trenches [4]:

$$I = \frac{H}{V}. \tag{9}$$

In Eq. (9), H refers to the horizontal etch depth or underetch, i.e., half the lateral extent of the trench at the top minus half the initial mask opening; and V refers to the vertical etch depth. These quantities are shown in Fig. 7. In ideally isotropic structures $I = 1$, while fully anisotropic vertical structures result in $I = 0$. This degree of isotropy has to be precisely controlled by the process recipe, even if the desired outcome is not necessarily $I = 1$. For example, for laser cavity applications, a process with I near 1 would result in a flat bottom which is an undesirable feature [30].

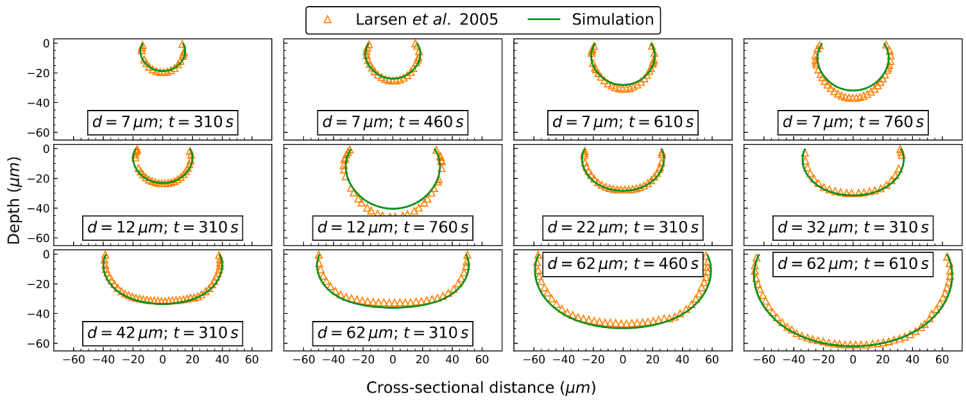

Fig. 5. Comparison of simulation results to trench profiles reported by Larsen et al. [13] for multiple photoresist openings d and etch times t using the same simulation parameter set from Table 5. The simulated profiles with $t \geqslant 610\,s$ show a slight underestimation of the local etch rates since our model does not include the effects of photoresist bending.

Table 5
Calibrated parameter set for trench profiles reported by Larsen et al. [13].

Parameter	Calibrated value
ER_{Si}	7.80 μm min^{-1}
ER_{resist}	0.0 μm min^{-1}
β_{Si}	35%
β_{resist}	6.1%

Table 6
Calibrated parameter set for trench geometry reported by Panduranga et al. [4].

Parameter	Calibrated value
ER_{Si}	2.40 μm min^{-1}
$ER_{hardmask}$	0.0 μm min^{-1}
β_{Si}	50%
$\beta_{hardmask}$	5%

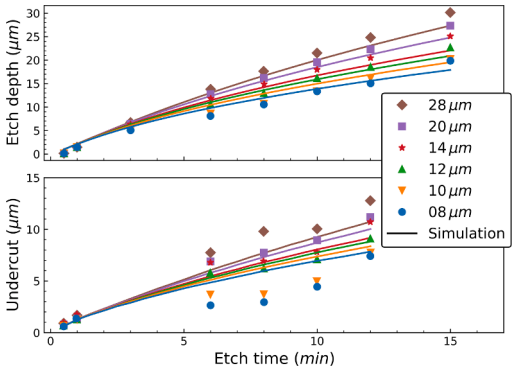

Fig. 6. Time evolution of the undercut and etch depth for trenches with different openings. The points refer to the reported values by Panduranga et al. [4] and the solid lines are simulation results.

Therefore, we are driven to apply our phenomenological model to improve the understanding of the nature of isotropy in features. In this section, we explore how the model parameters affect the degree of isotropy by means of computational experiments. To this end, we aim to develop an empirical relationship between the model parameters and I which can be of use for etch process engineers.

As discussed in Section 3, our phenomenological model accurately describes different trench profiles in the same reactor configuration with a single parameter set. However, we observe in Tables 2, 5, and 6 that each reactor configuration yields a distinct parameter set. For that reason, we assume that the model parameters serve as a proxy for the reactor configuration. Thus, we perform a computational study of the dependence of I with ER_{Si}, β_{Si}, etch time, and geometrical parameters. These different parameters represent multiple possible experimental configurations.

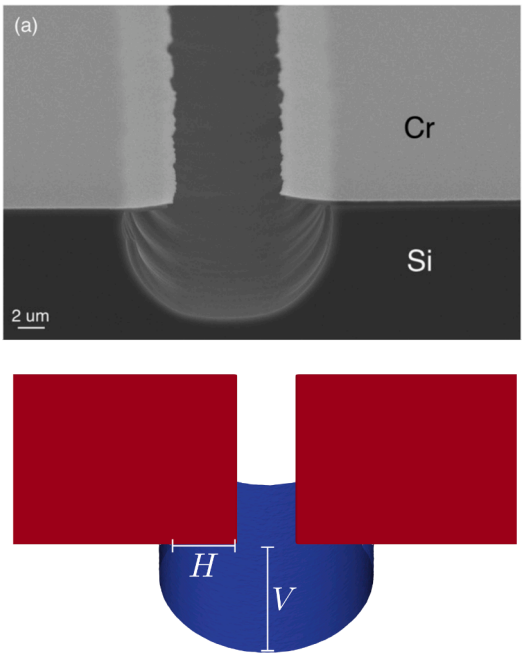

Fig. 7. Comparison of simulated topography to scanning electron microscopy image from Panduranga et al. [4] for a trench with $d = 8$ μm. The undercut is shown by H and the etch depth by V. Reprinted with permission from J. Vac. Sci. Technol. B 37, 061206 (2019). Copyright 2019, American Vacuum Society.

We start our computational experiment with the calibrated parameters from Table 6 and a trench with $d = 12$ μm. With a fixed plane-wafer etch rate of $ER_{Si} = 2.40\,\mu m\,min^{-1}$, we run the simulation for a total etch time of 1 h for a sweep of values of β_{Si} from 0 to 1. We then extract the degree of isotropy I every $30\,s$ and plot the results in a heat map in Fig. 8. Additionally, we plot only the contour map of I for a trench with $d = 60$ μm. The data from this heat map can be used by experimental setups with different plane-wafer etch rates, as long as the time axis is scaled accordingly.

In Fig. 8 we note that, as observed in the original work [4], I is

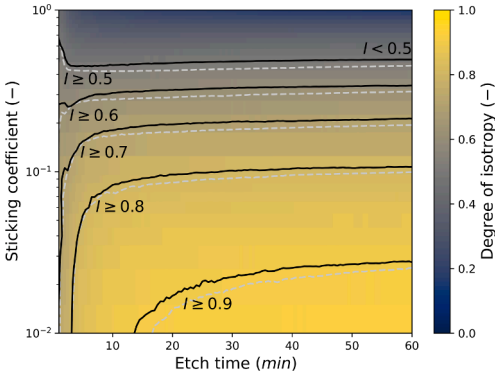

Fig. 8. Heat map of simulated degree of isotropy (I) as a function of the sticking coefficient and etch time for trenches with $d = 12$ µm and $ER_{Si} = 2.40$ µm min^{-1}. Simulation parameters from Table 6. The grey line shows I contours for trenches with $d = 60$ µm.

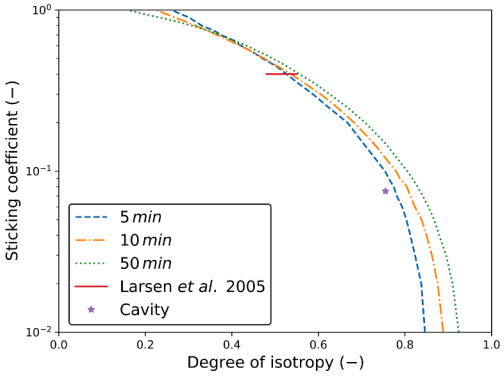

Fig. 9. Empirical relationship between sticking coefficient β and the degree of isotropy I for multiple etch times. The line indicated with "Larsen et al. 2005" shows the range of I extracted from reported profiles [13] and the calibrated β. The point indicated with "Cavity" depicts the calibrated β as a function of I measured after the first simulated etch step of the cavity presented in Section 3.1.

impacted by the change of mask width only in a very limited way. We also observe that after an initial saturating period, the degree of isotropy changes little with time. Thus, our simulation study indicates that both the sticking coefficient and I are strongly linked and are essentially constant for a given reactor configuration.

By fixing the etch times to 5, 10, and 50 min, we can extract an empirical relationship between the sticking coefficient and I. The result is shown in Fig. 9. This relationship is useful since the degree of isotropy is a quantity which is directly observable experimentally, whereas the phenomenological sticking requires either the calibration of simulations or complex experiments. That is, a process engineer can use this empirical relationship to estimate the sticking coefficient from an experimental measurement of I. Alternatively, these results are also important for users of topography simulation wishing to speed up the calibration process by making an educated guess of the expected sticking value.

To show the usefulness of the empirical relationship from Fig. 9, we also show the range of values of I extracted from profiles reported by Larsen et al. [13] and our manual independent calibration of β_{Si} discussed in Section 3.3. These values show good agreement to the empirical relationship, emphasizing that the measured I provides a starting point for estimations of the sticking. In addition, we present the simulated I for the cavities described in Section 3.1 after the first etch step with their automatically calibrated sticking coefficient. This accentuates the value of the method, since it provides an alternative to the automated calibration. However, the deviations present can be accounted by their different geometry, i.e., a cylindrical hole and not a trench.

As discussed in Section 2.2, our phenomenological sticking coefficient does not necessarily correspond directly to the true F reaction probability. Still, we expect that if a reduction in reaction probability is measured, a reduction in the sticking coefficient must follow. In a recent review of F-based plasma etching of Si [19], it has been shown that the reaction rate of F greatly diminishes with an increase of the measured flux of F Γ_F. Therefore, if an etch process engineer measures a degree of isotropy which is insufficient for the desired targets, the reactor configuration should be adapted paying attention to the expected changes in Γ_F. The chuck temperature is another reactor configuration parameter known to have an impact on the chemical reaction paths and their probabilities [19]. A distinct reactor configuration would then require a new estimation of the phenomenological sticking for further fine-tuning of the recipe.

5. Conclusion

We present a feature-scale topography simulation with a top-down flux calculation approach tailored to the challenges of low-bias SF_6 plasma etching of Si. Particular attention is placed to the involved phenomenological surface model and its key parameter: the average effective sticking coefficient. By contrasting it to conventional models, we show that our phenomenological model is more suited to simulating the final etched surfaces. We discuss how the effect of reactor loading can be included as a general reduction of the etch rates. Through calibrating our model to two different experiments reported in the literature, we emphasize that our model can reproduce multiple geometries and etch times in the same reactor configuration with the same parameter set.

Thus, we conclude that the reactor configuration can be captured in a phenomenological way by the model parameters, in particular, by the average effective sticking coefficient. By way of a series of computational experiments, we construct an empirical relationship between the average effective sticking coefficient and the degree of isotropy I (Fig. 9). Since I can be measured experimentally, we propose that it can be used to estimate the average effective sticking coefficient, thereby avoiding unnecessary calibration steps or complex experiments. Finally, since we expect that the average effective sticking coefficient is mainly influenced by the F flux Γ_F, we submit that our empirical relationship can be used in practice in order to fine-tune the desired degree of isotropy.

Declaration of Competing Interest

The authors declare that they have no known competing financial interests or personal relationships that could have appeared to influence the work reported in this paper.

Acknowledgement

The financial support by the Austrian Federal Ministry for Digital and Economic Affairs, the National Foundation for Research, Technology and Development and the Christian Doppler Research Association is gratefully acknowledged. M. Trupke and G. Wachter gratefully acknowledge support from the EU H2020 framework programme (QuanTELCO, 862721), the FWF (SiC-EiC, I 3167-N27), and the FFG (QSense4Power, 877615). The authors acknowledge TU Wien Bibliothek for financial support through its Open Access Funding Program.

References

[1] Donnelly VM, Kornblit A. Plasma etching: yesterday, today, and tomorrow. J Vacuum Sci Technol A: Vacuum Surfaces Films 2013;31(5):050825. https://doi.org/10.1116/1.4819316.

[2] Waits C, Morgan B, Kastantin M, Ghodssi R. Microfabrication of 3D silicon MEMS structures using gray-scale lithography and deep reactive ion etching. Sens Actuat A: Phys 2005;119(1):245–53. https://doi.org/10.1016/j.sna.2004.03.024.
[3] Patocka F, Schneidhofer C, Dörr N, Schneider M, Schmid U. Novel resonant mems sensor for the detection of particles with dielectric properties in aged lubricating oils. Sens Actuat A: Phys 2020;315:112290. https://doi.org/10.1016/j.sna.2020.112290.
[4] Panduranga P, Abdou A, Ren Z, Pedersen RH, Nezhad MP. Isotropic silicon etch characteristics in a purely inductively coupled SF_6 plasma. J Vacuum Sci Technol B, Nanotechnol Microelectron: Mater, Processing Meas, Phenomena 2019;37(6):061206. https://doi.org/10.1116/1.5116021.
[5] Lieberman MA, Lichtenberg AJ. Principles of Plasma Discharges and Materials Processing. Hoboken, NJ: John Wiley & Sons; 2005.
[6] G. Wachter, S. Kuhn, S. Minniberger, C. Salter, P. Asenbaum, J. Millen, M. Schneider, J. Schalko, U. Schmid, A. Felgner, et al., Silicon microcavity arrays with open access and a finesse of half a million, Light: Sci Appl 8 (1) (2019) 1–7. doi: 10.1038/s41377-019-0145-y.
[7] Rondé M, Walton AJ, Terry JG. Test structure for measuring the selectivity in XeF_2 and HF vapour etch processes. IEEE Trans Semicond Manuf 2021;34(3):241–7. https://doi.org/10.1109/TSM.2021.3063633.
[8] Flamm DL, Donnelly VM, Mucha JA. The reaction of fluorine atoms with silicon. J Appl Phys 1981;52(5):3633–9. https://doi.org/10.1063/1.329098.
[9] Coburn JW, Winters HF. Ion-and electron-assisted gas-surface chemistry–an important effect in plasma etching. J Appl Phys 1979;50(5):3189–96. https://doi.org/10.1063/1.326355.
[10] van Erp R, Soleimanzadeh R, Nela L, Kampitsis G, Matioli E. Co-designing electronics with microfluidics for more sustainable cooling. Nature 2020;585(7824):211–6. https://doi.org/10.1038/s41586-020-2666-1.
[11] Madou MJ. Manufacturing Techniques for Microfabrication and Nanotechnology, vol. 2. Boca Raton, FL: CRC Press; 2011.
[12] Hays DC, Jung KB, Hahn YB, Lambers ES, Pearton SJ, Donahue J, Johnson D, Shul RJ. Comparison of F_2-based gases for high-rate dry etching of Si. J Electrochem Soc 1999;146(10):3812–6. https://doi.org/10.1149/1.1392556.
[13] Larsen KP, Ravnkilde JT, Hansen O. Investigations of the isotropic etch of an icp source for silicon microlens mold fabrication. J Micromech Microeng 2005;15(4):873–82. https://doi.org/10.1088/0960-1317/15/4/028.
[14] Larsen KP, Petersen DH, Hansen O. Study of the roughness in a photoresist masked, isotropic, SF_6-nased icp silicon etch. J Electrochem Soc 2006;153(12):G1051. https://doi.org/10.1149/1.2357723.
[15] Biedermann GW, Benito FM, Fortier KM, Stick DL, Loyd TK, Schwindt PDD, Nakakura CY, Jarecki RL, Blain MG. Ultrasmooth microfabricated mirrors for quantum information. Appl Phys Lett 2010;97(18):181110. https://doi.org/10.1063/1.3511743.
[16] Klemenschits X, Selberherr S, Filipovic L. Modeling of gate stack patterning for advanced technology nodes: a review. Micromachines 2018;9(12):631. https://doi.org/10.3390/mi9120631.
[17] Belen RJ, Gomez S, Kiehlbauch M, Cooperberg D, Aydil ES. Feature-scale model of Si etching in SF_6 plasma and comparison with experiments. J Vacuum Sci Technol A: Vacuum Surfaces Films 2005;23(1):99–113. https://doi.org/10.1116/1.1830495.
[18] Aguinsky LF, Wachter G, Manstetten P, Rodrigues F, Trupke M, Schmid U, Hössinger A, Weinbub J. Modeling and analysis of sulfur hexafluoride plasma etching for silicon microcavity resonators. J Micromech Microeng 2021;31(12):125003. https://doi.org/10.1088/1361-6439/ac2bad.
[19] Donnelly VM. Reactions of fluorine atoms with silicon, revisited, again. J Vacuum Sci Technol A: Vacuum Surfaces Films 2017;35(5):05C202. https://doi.org/10.1116/1.4983922.
[20] Arora P, Nguyen T, Chawla A, Nam S-K, Donnelly VM. Role of sulfur in catalyzing fluorine atom fast etching of silicon with smooth surface morphology. J Vacuum Sci Technol A: Vacuum Surfaces Films 2019;37(6):061303. https://doi.org/10.1116/1.5125266.
[21] Manstetten P, Weinbub J, Hössinger A, Selberherr S. Using temporary explicit meshes for direct flux calculation on implicit surfaces. Procedia Comput Sci 2017;108:245–54. https://doi.org/10.1016/j.procs.2017.05.067.
[22] Sethian JA. Level Set Methods and Fast Marching Methods: Evolving Interfaces in Computational Geometry, Fluid Mechanics, Computer Vision, and Materials Science. Cambridge: Cambridge University Press; 1999.
[23] Silvaco, Victory Process (2021). url: www.silvaco.com/tcad/victory-process-3d/.
[24] Vienna TS. Available online: url: https://github.com/viennats/viennats-dev (accessed on 15 October 2021).
[25] Williams KR, Gupta K, Wasilik M. Etch rates for micromachining processing-part II. J Microelectromech Syst 2003;12(6):761–78. https://doi.org/10.1109/JMEMS.2003.820936.
[26] Miao J. Silicon Micromachining. US, Boston, MA: Springer; 2008. p. 1840–6.
[27] Kokkoris G, Boudouvis AG, Gogolides E. Integrated framework for the flux calculation of neutral species inside trenches and holes during plasma etching. J Vacuum Sci Technol A: Vacuum Surfaces Films 2006;24(6):2008–20. https://doi.org/10.1116/1.2345643.
[28] Kleckner D, Irvine WT, Oemrawsingh SS, Bouwmeester D. Diffraction-limited high-finesse optical cavities. Phys Rev A 2010;81(4):043814. https://doi.org/10.1103/PhysRevA.81.043814.
[29] Mogab C. The loading effect in plasma etching. J Electrochem Soc 1977;124(8):1262–8. https://doi.org/10.1149/1.2133542.
[30] D.A. Steck, Classical and Modern Optics, Available online: url: http://steck.us/teaching (revision 1.8.3, 25 July 2021, accessed on 04 November 2021).

Luiz Felipe Aguinsky was born in 1990 in Porto Alegre, Brazil. He received his Bachelor's degree in Physics from the Federal University of Rio Grande do Sul (BSc, 2013). Subsequently, he studied Simulation Sciences at RWTH Aachen University (MSc, 2018), having written the Master's thesis at the German Aerospace Center. After finishing his studies he joined the Institute for Microelectronics at TU Wien in March 2018, where he is currently working on his doctoral degree. He is researching high performance numerical approaches for Technology CAD within the scope of the Christian Doppler Laboratory for High Performance TCAD.

Frâncio Souza Berti Rodrigues was born in 1991 in Caxias do Sul, Brazil. He received his Bachelor's degree in Engineering Physics from the Federal University of Rio Grande do Sul (BSc, 2015). Subsequently, he received his Master's Degree in Microelectronics from the same university (MSc, 2018). After finishing his studies, he worked in research and development for the semiconductor packaging industry before joining the Institute for Microelectronics at TU Wien in September 2019. He is currently pursuing his doctoral degree, researching high performance numerical approaches for Technology CAD within the scope of the Christian Doppler Laboratory for High Performance TCAD.